Coupled Rotor-Fuselage Analysis with Finite Motions Using Component Mode Synthesis*

Olivier A. Bauchau and Jesus Rodriguez
School of Aerospace Engineering,
Georgia Institute of Technology,
Atlanta, GA, USA.
Shyi-Yaung Chen
Research and Engineering,
Sikorsky Aircraft, Stratford, CT, USA.

Abstract

This paper is concerned with the modeling of a rotor-fuselage system undergoing large angle maneuvers. The behavior of the elastic fuselage will be represented by a modal approximation, thereby greatly reducing the computational cost of the simulation. In this work, a floating frame approach is used. The total motion of the fuselage consists of the superposition of the rigid body motions of the floating frame and of elastic motions that are assumed to remain small. The proposed formulation makes use of a component mode synthesis technique that leaves the analyst free to choose any type of modal basis and simplifies the connection of the fuselage to other rotorcraft components. The proposed formulation is independent of the finite element analysis package used to compute the modes of the fuselage. It is also shown that in the absence of elastic deformations, the formulation recovers the exact equations of motion for a rigid body.

1 Introduction

Rotorcraft vibration analyses often assume the hub to be attached to an inertial point. While this convenient approximation considerably simplifies the analysis, it implies that rotor and fuselage responses are fully decoupled. In reality, airframe motion is known to have a significant impact on hub loads, see Refs. [1, 2]. Consequently, a comprehensive rotorcraft dynamics analysis requires the coupling of a realistic fuselage model to a nonlinear rotor model. Helicopters and tilt-rotors perform complex, highly dynamic and often three-dimensional maneuvers, both in normal operating conditions and during emergencies. The ability to perform aggressive and violent maneuvers is clearly a primary goal of rotorcraft systems designed for military applications. In fact, limits on the maneuvers a rotorcraft can fly might arise not from the ability of the rotor system to generate the desired thrust, but on the ability of critical dynamic components to carry the resulting loads. Hence, coupled rotor/fuselage models are needed for hover, forward flight, and maneuvers.

Various methods have been proposed for the study of rotor-fuselage interactions. The impedance matching method was implemented to couple and solve rotor and fuselage dynamics (Refs. [3, 4]). Reference [5] derived a set of dynamic equations of motion for a rotor-fuselage system which was

Journal of the American Helicopter Society, **49**(2), pp 201– 211, 2004

solved by means of the harmonic balance technique. Stephens and Peters (Ref. [6]) presented both an iterative method and a fully coupled method to predict the response a rotor-body system. Bir and Chopra (Ref. [7]) studied the dynamic response of a rotor/rigid fuselage system subjected to a three-dimensional gust. References [8, 2] derived a comprehensive set of rotor-body equations for the analysis of the Bell AH-1G helicopter. Many of these approaches assume small amplitude rigid body motions of the fuselage, rendering them inapplicable to large angle maneuver flights. Other techniques require the reformulation of the blade equations of motion, a cumbersome task. Modal approximation seems to be the method of choice for representing the elasticity of the fuselage, leading to manageable computational costs. The diversity of the approaches and their underlying assumptions underscore the difficulties associated with the formulation and solution of this complex problem.

Modal based approximations of complex elastic substructures have been widely used within the framework of multibody dynamics. One of the most common approaches is based on the concept of floating frames (Refs. [9, 10]) whereby the total motion of a flexible body is broken into two parts: rigid body motions represented by the motion of the floating frame, and superimposed "elastic motions." This decomposition allows the introduction of simplifying assumptions: although the total motion is always finite, the elastic motions remain small. In forward flight, the rigid body motion simply is a forward translation, but in maneuver flight, large angle motion will be encountered. In both cases, elastic motions are assumed to be small. The focus of this paper is the formulation of modal based elements that can be used to model coupled rotor/fuselage problems in hover, forward flight and maneuvers, within the framework of finite element based, nonlinear flexible multibody dynamics formulations.

Although the concept of floating frame is rather intuitive, the implementation of a computational procedure based on this idea must deal with several thorny issues. First, the accuracy of the analysis will critically depend on the selection of a suitable modal basis. Second, a specific floating frame must be selected: it could be attached to a point of the elastic body or moving with respect to it. Third, the modal based elements should be easy to couple with the other components of the system modeled with multibody formulations. This points towards the use of component mode synthesis techniques that are well developed for structural dynamics problems. Fourth, in the absence of elastic deformations, the formulation should recover the exact equations of motion for a rigid body. Finally, the formulation should be independent of the finite element analysis package used to compute the modes of the elastic components; any commercial finite element package could be used, and the resulting modal based element can be used independently of the commercial package. These various issues will be discussed in more detail in the following paragraphs.

The first critical step is the selection of a suitable modal basis. Ideally, the selected modes should capture as accurately as possible the deformation patterns encountered during flight. Consequently, the analyst should be given the greatest possible freedom to select appropriate modes. The formulation should not put any restriction on the choice of the modal basis. In particular, the modes near integer multiples of the blade passage frequency should be included in the analysis. Since such modes will not be the lowest frequency modes of the fuselage, a highly detailed finite element model must be used. The DAMVIBS program (Ref. [11]) describes the results of some of the research efforts in this area.

Next, a specific floating frame must be selected. Since there exists no unique manner of defining the "rigid" and "elastic" motions, the floating frame can be selected in a number of different ways. Several authors make use of body-attached frames, *i.e.* the floating frame is attached to an arbitrary point in the body (Refs. [12, 13, 14]). Other authors rely on floating frames moving with respect to the elastic body (Refs. [15, 16]). Since the choice of the location of the moving frame is not unique, a specific condition must be selected to remove this indeterminacy. For instance, one can choose to minimize the kinetic energy (Ref. [15]), to place the frame at the mass center of the structure (Ref. [16]), or follow the center-of-mass/mean axis convention used for rotorcraft modeling (Ref. [5]).

The choice of one condition or the other seems to be a matter of computational convenience. The moving frame approach seems to be more desirable than the body-attached approach because it eliminates the need to arbitrarily select a material point where to attach the floating frame. On the other hand, the moving frame approach also involves the analyst's insight since a specific condition must be selected to determine its location. Furthermore, this latter approach comes at the expense of additional computational complexity. In this work, a body-attached frame will be used.

In some formulations, the choice of the floating frame is intimately linked to that of the modes used in the reduction technique (Refs. [17, 18, 9]). This linkage hinders the selection of the most appropriate modes because the boundary conditions used to compute them do not necessarily match those of the flexible component once it is part of a multibody system.

An important issue in the formulation is the coupling of the modal based element representing the fuselage to the rotor, tail rotor and landing gear. In the classical application of modal analysis (Ref. [19]), the displacement field is represented as a linear combination of mode shapes. This type of representation has been used by some authors (Ref. [20]) in the context of multibody dynamics analysis, but it requires special techniques for coupling the modal based element with the other components of the system. Typically, this is done by formulating a constraint condition that equates the modal superposition to the physical displacement at a node of the model (Ref. [21]). However, this approach does not take advantage of the component mode synthesis techniques that have been developed for structural dynamics problems over the past thirty years. In these approaches, the model of the fuselage involves two types of degrees of freedom: physical degrees of freedom at a limited number of connection points (called "boundary nodes") and modal degrees of freedom representing its internal flexibility. The fuselage is then readily connected at the boundary nodes to the main and tail rotors or landing gear without resorting to complex coupling techniques. Among the most widely used component mode synthesis techniques are those of Craig and Bampton (Ref. [22]), MacNeal (Ref. [23]), Rubin (Ref. [24]). Other efforts include those of Herting (Ref. [25]), Hintz (Ref. [26]) and refinements of the Craig-Bampton method (Ref. [27]).

Component mode synthesis methods were first used in the context of multibody dynamics by Haug and coworkers (Refs. [28, 29, 30, 31]) and later by Cardona and coworkers (Refs. [13, 14, 16]) who used the Craig-Bampton method. Unfortunately, this method requires the use of modes associated with clamped conditions at the boundary nodes: *i.e.* the modal basis must be selected among the modes of the fuselage *clamped* at the main and tail rotor connections and landing gear connection. This would clearly lead to a poor representation of fuselage flexibility. This fundamental limitation of the approach was recognized by Craig and Bampton who suggested the use of "static correction modes" to alleviate the problem. It also prompted the development of the MacNeal-Rubin method. However, in this case, free conditions must be used at all boundary nodes: the modal basis must be select from among the modes of the *unconstrained* fuselage *excluding* the main and tail rotors and landing gear. Furthermore, this method is more cumbersome to implement than the Craig-Bampton method; it seems that the MacNeal-Rubin method has not been used in conjunction with multibody formulations. Finally, Herting's method offers a more general approach that enables the analyst to choose *any* type of modes. In fact, predictions based on the Craig-Bampton and MacNeal-Rubin methods were found to be in good agreement with those obtained from Herting's method (Ref. [25]). In this work, Herting's method will be used as it provides the analyst maximum flexibility.

The formulation of modal based elements should be independent of the finite element analysis package used to compute the modes of the elastic components (Refs. [28, 29, 13, 14, 16]). This means that the computation of the mass and stiffness coefficients used for the formulation of a modal based element should be solely based on the information readily provided by the finite element package. Typically, rotorcraft companies develop very sophisticated fuselage models using commercial finite element packages (Ref. [11]); these models involve hundreds of thousands of degrees of freedom. The formulation of the modal based element should require some basic information provided by these

models, such as the linearized mass and stiffness matrices, but it should not require additional data. Some formulations have been proposed in which the finite element analysis tool is embedded in the multibody formulation (Ref. [32]). Although higher accuracy can be achieved in that manner, this is clearly not a practical option when a realistic finite element model of a fuselage is used. Yoo and Haug (Ref. [28, 29]) showed that by assuming a lumped mass representation of the elastic body, the modal based formulation could be fully decoupled from the finite element package. Unfortunately, the lumped mass approximation is rarely used for realistic fuselage models. Cardona and Géradin (Refs. [13, 14, 16]) used a corotational technique to achieve the same decoupling without resorting to the lumped mass approximation.

The proposed modal based element for fuselage dynamics modeling is fully independent of the finite element analysis package. The mass and stiffness coefficients of the element are computed on the sole basis of the unconstrained mass and stiffness matrices of the elastic fuselage and Herting's transformation. Existing finite element models of fuselages can be readily used to generate the modal based element. It is also shown that Herting's transformation applies to the inertial velocities required to compute the kinetic energy of the elastic component, under the sole assumption of small displacements.

The paper is organized in the following manner. After a brief discussion of the notational conventions used in this work, the component mode synthesis technique presented by Herting (Ref. [25]) is briefly reviewed. Next, the modal based multibody formulation is described. Finally, the last section presents numerical examples to validate the proposed formulation.

2 Notational Conventions

The kinematic description of bodies in their reference and deformed configurations will make use of three orthonormal bases. First, an inertial basis is used as a global reference for the system; it is denoted $\mathcal{I} := (\bar{\imath}_1, \bar{\imath}_2, \bar{\imath}_3)$, the over-bar indicates a unit vector. A second basis $\mathcal{B}^0 := (\bar{e}_{01}, \bar{e}_{02}, \bar{e}_{03})$, is attached to the body and defines its orientation in the reference configuration. Finally, a third basis $\mathcal{B} := (\bar{e}_1, \bar{e}_2, \bar{e}_3)$ defines the orientation of the body in its deformed configuration.

Let $\underline{u}_0$ and $\underline{u}$ (under-bars indicate vector quantities) be the displacement vectors from $\mathcal{I}$ to $\mathcal{B}^0$ and $\mathcal{B}^0$ to $\mathcal{B}$, respectively, and R_0 and R the rotation tensors from $\mathcal{I}$ to $\mathcal{B}^0$ and $\mathcal{B}^0$ to $\mathcal{B}$, respectively. In this work, all vector and tensor components are measured in either $\mathcal{I}$ or $\mathcal{B}$. For instance, the components of vector $\underline{u}$ measured in $\mathcal{I}$, and $\mathcal{B}$ will be denoted $\underline{u}$, and $\underline{u}^*$, respectively, and clearly

$$\underline{u}^* = (RR_0)^T \, \underline{u}. \tag{1}$$

Similarly, the components of tensor R measured in $\mathcal{I}$ and $\mathcal{B}$ will be denoted R and R^*, respectively. The notation $(.)^T$ denotes the transposition of a vector of matrix. The skew-symmetric matrix formed with the components $\underline{u}$ will be denoted $\tilde{u}$

$$\tilde{u} = \begin{bmatrix} 0 & -u_3 & u_2 \\ u_3 & 0 & -u_1 \\ -u_2 & u_1 & 0 \end{bmatrix}. \tag{2}$$

3 Herting's Transformation

Consider an elastic fuselage whose linearized equations of motion are in the following form

$$M\ddot{\underline{\hat{u}}}^* + K\underline{\hat{u}}^* = \underline{\hat{F}}(t), \tag{3}$$

where $\underline{\hat{u}}^*(t)$ is the array of nodal displacements and rotations, $\underline{\hat{F}}(t)$ the array of externally applied nodal forces, K and M the unconstrained stiffness and mass matrices of the fuselage, respectively,

and t time. The notation $\hat{(.)}$ is used to denote the nodal values of quantities discretized using finite element procedures. For three dimensional problems, matrix K is six times singular, corresponding to the six rigid body modes of the fuselage. The structure is assumed to be undamped or lightly damped and hence, damping effects are neglected. Eqs. (3) forms a large set of N algebraic equations, typically obtained from a spatial discretization process such as the finite element method. Let matrix P store all the mass normalized eigenmodes of the fuselage in order of ascending frequencies

$$P = [P_R, P_E]\,, \tag{4}$$

where $P_R = \left[\underline{u}_1, \underline{u}_2, \ldots \underline{u}_{N_R}\right]$ stores the N_R rigid body modes of the structure and $P_E = \left[\underline{u}_{N_R+1}, \underline{u}_{N_R+2}, \ldots \underline{u}_N\right]$ its $N - N_R$ elastic modes.

The aim of this work is to develop a modal approximation to the elastic component (fuselage) represented by eqs. (3) which will be connected to other components (main and tail rotor, landing gear) to form the complete system (rotorcraft) to be analyzed. The other components could be modeled by a modal representation, or by a multibody formulation. In order to allow the connection of a specific component to others, its degrees of freedom will be partitioned into boundary and interior degrees of freedom, denoted $\underline{d}^{B*}$ and $\underline{\hat{u}}^{I*}$, respectively. The array $\underline{d}^{B*T} = \lfloor \underline{d}_1^{B*T}, \underline{d}_2^{B*T}, \ldots \underline{d}_m^{B*T} \rfloor$ stores the six degrees of freedom for each of the m boundary points of the component. Each boundary point requires six degrees of freedom, three displacements and three rotations, for compatibility with multibody formulations, *i.e.* $\underline{d}_i^{B*T} = \lfloor \underline{u}_i^{B*T}, \underline{\theta}_i^{B*T} \rfloor$. The following partition of the structural matrices is performed

$$M = \begin{bmatrix} M^{BB} & M^{BI} \\ M^{IB} & M^{II} \end{bmatrix}; \quad K = \begin{bmatrix} K^{BB} & K^{BI} \\ K^{IB} & K^{II} \end{bmatrix}, \tag{5}$$

$$\underline{\hat{u}}^* = \begin{bmatrix} \underline{d}^{B*} \\ \underline{\hat{u}}^{I*} \end{bmatrix}; \quad \underline{\hat{F}}(t) = \begin{bmatrix} \underline{F}^B(t) \\ \underline{\hat{F}}^I(t) \end{bmatrix}, \tag{6}$$

and

$$P_R = \begin{bmatrix} P_R^B \\ P_R^I \end{bmatrix}; \quad P_E = \begin{bmatrix} P_E^B \\ P_E^I \end{bmatrix}, \tag{7}$$

where the superscripts $(\cdot)^B$ and $(\cdot)^I$ denoted the boundary and interior degrees of freedom, respectively. It is assumed that the partition K^{II} is nonsingular.

Herting (Ref. [25]) introduced a coordinate transformation

$$\underline{\hat{u}}^* = H_H\, \underline{\bar{u}}, \tag{8}$$

defined by a set of shape functions H_H

$$H_H = \begin{bmatrix} I & 0 & 0 \\ G^{IB} & H_R^I & P_E^I - G^{IB} P_E^B \end{bmatrix}, \tag{9}$$

where

$$G^{IB} = -K^{II-1} K^{IB}, \tag{10}$$

$$H_R^I = -K^{II-1} \left(M^{IB} + M^{II} G^{IB}\right) P_R^B. \tag{11}$$

The reduced set of degrees of freedom is

$$\underline{\bar{u}}^T = \lfloor \underline{d}^{B*T},\ \underline{q}_R^T,\ \underline{q}_E^T \rfloor, \tag{12}$$

where $\underline{q}_R$ and $\underline{q}_E$ correspond to the modal participation factors for the rigid and elastic modes, respectively.

In the absence of interior loads, *i.e.* when $\underline{\hat{F}}^I(t) = 0$, the equations of motion, eqs. (3), reduce to

$$\bar{M}\,\underline{\ddot{\bar{u}}} + \bar{K}\,\underline{\bar{u}} = \underline{\bar{F}}, \tag{13}$$

where

$$\bar{M} = H_H^T M H_H; \quad \bar{K} = H_H^T K H_H; \quad \underline{\bar{F}} = H_H^T \underline{\hat{F}}(t). \tag{14}$$

Typically, boundary degrees of freedom and modal coordinates are coupled in the reduced mass matrix $\bar{M}$, whereas the reduced stiffness matrix takes the following form

$$\bar{K} = \begin{bmatrix} \bar{K}^{BB} & 0 \\ 0 & \bar{K}^{qq} \end{bmatrix}, \tag{15}$$

where $\bar{K}^{BB}$ is the partition obtained from a Guyan (Ref. [33]) reduction and the superscript $(.)^q$ refers to the modal coordinates. Clearly, boundary degrees of freedom and modal coordinates are statically uncoupled. In general, damping effect are not represented in finite element models; finite element codes provide a mass and a stiffness matrix but no damping matrix in eq. (3). Hence, component mode synthesis is typically performed for undamped systems. However, once the reduction has been performed to obtain the reduced mass and stiffness matrices, eq. (14), a modal damping matrix can be added to the model, often based on experimental measurements of modal damping.

4 Multibody Formulation

In this section, the kinematics of the modal based element are presented. The proposed formulation follows the floating frame approach, where small elastic displacements and rotations are superimposed with the large rigid body motion of the elastic body. Expressions for the kinetic and strain energies are then derived.

4.1 Modal Based Element Kinematics

Consider the elastic body shown in Fig. 1. The overall rigid body motion of the elastic fuselage is described by a floating frame the orientation of which is defined by the orthonormal bases $\mathcal{B}^{0F} := \left(\bar{e}^F_{01}, \bar{e}^F_{02}, \bar{e}^F_{03}\right)$ and $\mathcal{B}^F := \left(\bar{e}^F_1, \bar{e}^F_2, \bar{e}^F_3\right)$ in the reference and deformed configurations, respectively. Similarly, two additional orthonormal bases define the orientation of a frame rigidly attached to the fuselage at an arbitrary point $\mathbf{P}$, $\mathcal{B}^{0P} := \left(\bar{e}^P_{01}, \bar{e}^P_{02}, \bar{e}^P_{03}\right)$ and $\mathcal{B}^P := \left(\bar{e}^P_1, \bar{e}^P_2, \bar{e}^P_3\right)$ in the reference and deformed configurations, respectively. R^F_0 and R^F are the components of the rotation tensors from the inertial frame $\mathcal{I}$ to $\mathcal{B}^{0F}$ and $\mathcal{B}^{0F}$ to $\mathcal{B}^F$, respectively, both measured in $\mathcal{I}$. Similarly, R^P_0 and R^P are the components of the rotation tensors from $\mathcal{I}$ to $\mathcal{B}^{0P}$ and $\mathcal{B}^{0P}$ to $\mathcal{B}^P$, respectively, both measured in $\mathcal{I}$. In the reference configuration, the origin of the floating and body-attached frames are denoted by $\underline{x}^F_0$

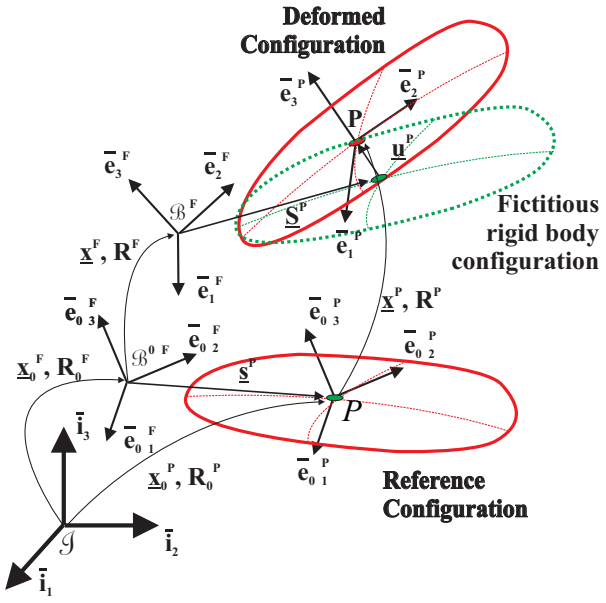

Figure 1: Configuration of the elastic body.

and $\underline{x}_0^P$, respectively. The position vector $\underline{s}^P$ of point **P** with respect to the floating frame vector is $\underline{s}^P = \underline{x}_0^P - \underline{x}_0^F$. The orientations of the floating and body-attached frames are identical in the reference configuration, *i.e.* $R_0^F = R_0^P = R_0$. The displacement vectors of the floating and body-attached frames are denoted $\underline{x}^F$ and $\underline{x}^P$, respectively.

The total motion of the elastic fuselage consists of the superposition of a rigid body motion and an elastic motion. The rigid body motion, defined by the motion of the floating frame, brings the fuselage to the "fictitious rigid body configuration" shown in Fig. 1. Since this motion is rigid, the position vector of point **P** with respect to the floating frame, measured in this frame, remains unchanged, *i.e.* $\underline{s}^{P*} = \underline{S}^{P*}$, where $\underline{s}^{P*} = R_0^T\,\underline{s}^P$, $\underline{S}^{P*} = (R^F R_0)^T\,\underline{S}^P$, and $\underline{S}^P$ denotes the position vector of point **P** in the fictitious rigid body configuration. The position of point **P** is now written as

$$\underline{x}_0^P + \underline{x}^P = \underline{x}_0^F + \underline{x}^F + \underline{S}^P + \underline{u}^P = \underline{x}_0^F + \underline{x}^F + (R^F R_0)(\underline{s}^{P*} + \underline{u}^{P*}), \tag{16}$$

where $\underline{u}^P$ is the elastic displacement of the fuselage, and $\underline{u}^{P*} = (R^F R_0)^T\,\underline{u}^P$ the components of this displacement vector measured in frame $\mathcal{B}^F$. Solving eq. (16) then yields

$$\underline{u}^{P*} = (R^F R_0)^T \left(\underline{x}_0^P + \underline{x}^P - \underline{x}_0^F - \underline{x}^F\right) - \underline{s}^{P*}. \tag{17}$$

In general, the elastic fuselage also undergoes elastic rotations that will be defined in the following manner

$$\underline{\theta}^{P*} = \frac{1}{2}\begin{bmatrix} g_{32} - g_{23} \\ g_{13} - g_{31} \\ g_{21} - g_{12} \end{bmatrix} = \frac{1}{2}\begin{bmatrix} R^*_{32} - R^*_{23} \\ R^*_{13} - R^*_{31} \\ R^*_{21} - R^*_{12} \end{bmatrix} = \bar{n}^*\ \sin\phi, \tag{18}$$

where R^*_{ij} are the components of the relative rotation tensor $R^* = (R^F R_0)^T R^P R_0$; ϕ the magnitude of this relative rotation; $\bar{n}^*$ the unit vector about which it takes place; and $g_{\alpha\beta} = \bar{e}_\alpha^{FT}\ \bar{e}_\beta^P$. If the elastic displacements remain small, $\underline{\theta}^{P*} \approx \bar{n}^*\,\phi$ represents the infinitesimal rotation vector, although R^P and R^F both are finite rotations.

Since eqs. (17) and (18) are valid for any point on the elastic fuselage, they also hold for the boundary points, hence

$$\underline{u}^{B*} = (R^F R_0)^T \left(\underline{x}_0^B + \underline{x}^B - \underline{x}_0^F - \underline{x}^F\right) - \underline{s}^{B*}, \tag{19}$$

and

$$\underline{\theta}^{B*} = \frac{1}{2}\begin{bmatrix} g_{32} - g_{23} \\ g_{13} - g_{31} \\ g_{21} - g_{12} \end{bmatrix}, \tag{20}$$

where $g_{\alpha\beta} = \bar{e}_\alpha^{FT}\ \bar{e}_\beta^B$.

4.2 Strain Energy

With the help of Herting's transformation, eq. (8), the strain energy of the elastic body can be written as $\mathcal{V} = 1/2\ \bar{\underline{u}}^T \bar{K}\,\bar{\underline{u}}$. Using eqs. (19) and (20), the elastic forces $\underline{\mathcal{F}}^e$ are then readily found as

$$\delta\mathcal{V} = \begin{bmatrix} \delta\underline{x}^F \\ \delta\underline{\psi}^F \\ \delta\underline{x}^B \\ \delta\underline{\psi}^B \\ \delta\underline{q} \end{bmatrix}^T \begin{bmatrix} - & R^F R_0\ \underline{f}^u \\ - & T\,\underline{f}^\theta - \tilde{u}\,R^F R_0\,\underline{f}^u \\ & R^F R_0\ \underline{f}^u \\ & T\,\underline{f}^\theta \\ & \underline{f}^q \end{bmatrix} = \begin{bmatrix} \delta\underline{x}^F \\ \delta\underline{\psi}^F \\ \delta\underline{x}^B \\ \delta\underline{\psi}^B \\ \delta\underline{q} \end{bmatrix}^T \underline{\mathcal{F}}^e, \tag{21}$$

where

$$\begin{bmatrix} \underline{f}^u \\ \underline{f}^\theta \\ \underline{f}^q \end{bmatrix} = \bar{K}\begin{bmatrix} \underline{u}^{B*} \\ \underline{\theta}^{B*} \\ \underline{q} \end{bmatrix} \tag{22}$$

are elastic force components, and

$$\underline{q} = \begin{bmatrix} \underline{q}_R \\ \underline{q}_E \end{bmatrix}, \tag{23}$$

the array of modal participation factors. The following notations were introduced: $\underline{u} = \underline{x}_0^B + \underline{x}^B - \underline{x}_0^F - \underline{x}^F$; $T = 1/2\ [\underline{h}_{32} - \underline{h}_{23},\ \underline{h}_{13} - \underline{h}_{31},\ \underline{h}_{21} - \underline{h}_{12}]$, and $\underline{h}_{\alpha\beta} = \tilde{e}_\alpha^F\ \bar{e}_\beta^B$.

For simplicity of the exposition, the formulation was presented here for a single boundary point. The case of multiple boundary points is obtained by a straightforward generalization. The evaluation of the strain energy of the modal based element only requires the reduced stiffness matrix $\bar{K} = H_H^T K H_H$; hence, it is independent of the finite element code used to model the elastic fuselage.

4.3 Kinetic Energy

The total kinetic energy of the elastic body $\mathcal{K}$ is given by

$$\mathcal{K} = \frac{1}{2} \int_V \underline{\dot{x}}^{P*T} \underline{\dot{x}}^{*P}\, \rho \mathrm{d}V, \tag{24}$$

where $\dot{(.)} = \mathrm{d}(.)/\mathrm{dt}$; ρ is the material density, and V the volume of the elastic fuselage. For eq. (16), the inertial velocity, $\underline{\dot{x}}^P$, of an arbitrary point of the fuselage is

$$\underline{\dot{x}}^P = \underline{\dot{x}}^F + (\dot{R}^F R_0)\,(\underline{s}^{P*} + \underline{u}^{P*}) + (R^F R_0)\,\underline{\dot{u}}^{P*}. \tag{25}$$

Since the elastic displacements $\underline{u}^{P*}$ are assumed to remain small, this velocity is approximated by

$$\underline{\dot{x}}^P = \underline{\dot{x}}^F + (\dot{R}^F R_0)\,\underline{s}^{P*} + (R^F R_0)\,\underline{\dot{u}}^{P*}, \tag{26}$$

and its components measured in the floating frame become

$$\underline{\dot{x}}^{P*} = (R^F R_0)^T \underline{\dot{x}}^P = (R^F R_0)^T \underline{\dot{x}}^F + \tilde{\omega}^{F*} \underline{s}^{P*} + \underline{\dot{u}}^{P*} = \underline{v}_R^* + \underline{\dot{u}}^{P*}, \tag{27}$$

where $\underline{\omega}^{F*}$ is the angular velocity of the floating frame. The total velocity field is the superposition of the "rigid velocity" due to the floating frame motion, and the "elastic velocity", $\underline{\dot{u}}^{P*}$. This velocity field is now discretized in terms of nodal values $\underline{\hat{v}}^*$ with the help of interpolation functions

$$\underline{\dot{x}}^{P*} = H\, \underline{\hat{v}}^*, \tag{28}$$

where the matrix H stores the classical, finite element shape function (Ref. [34]). The kinetic energy now becomes

$$\mathcal{K} = \frac{1}{2}\, \underline{\hat{v}}^{*T} \left[\int_V H^T H\, \rho \mathrm{d}V \right] \underline{\hat{v}}^* = \frac{1}{2}\, \underline{\hat{v}}^{*T} M \underline{\hat{v}}^*, \tag{29}$$

where M is the mass matrix of the elastic fuselage, see eqs. (3).

Next, taking a time derivative of Herting's transformation, eq. (8), leads to

$$\begin{bmatrix} \underline{\dot{d}}^{B*} \\ \underline{\dot{\hat{u}}}^{I*} \end{bmatrix} = \begin{bmatrix} I & 0 \\ G^{IB} & H^{Iq} \end{bmatrix} \begin{bmatrix} \underline{\dot{d}}^{B*} \\ \underline{\dot{q}} \end{bmatrix}, \tag{30}$$

where $H^{Iq} = \left[H_R^I,\ P_E^I - G^{IB} P_E^B\right]$.

Consider now an array of nodal displacements, $\underline{\hat{u}}_R^*$, storing a rigid body mode of the elastic component. Partition (5) then implies $K^{IB}\, \underline{d}_R^{B*} + K^{II}\, \underline{\hat{u}}_R^{I*} = 0$, and hence $\underline{\hat{u}}_R^{I*} = G^{IB}\, \underline{d}_R^{B*}$ for any of the six rigid body modes. If the elastic component features a single boundary point, G^{IB} can

be interpreted as storing the value of rigid body motion at the interior points the elastic fuselage. Elementary kinematics for a rigid body then imply

$$\underline{\hat{v}}_R^{I*} = G^{IB}\,\underline{v}_R^{B*}, \tag{31}$$

where $\underline{\hat{v}}_R^{I*}$ and $\underline{v}_R^{B*} = \underline{\hat{v}}_R^{B*}$ are the rigid components of velocity at the interior and boundary nodes, respectively. Adding this relationship to eq. (30) then yields

$$(\underline{\hat{v}}_R^{I*} + \dot{\underline{\hat{u}}}^{I*}) = G^{IB}\,(\underline{v}_R^{B*} + \dot{\underline{d}}^{B*}) + H^{Iq}\,\dot{\underline{q}}. \tag{32}$$

In view of eq. (27), the terms between the first and second sets of parentheses represent the total velocity of an interior and boundary point, respectively. It follows that Herting's transformation, eq. (30), can be recast as

$$\begin{bmatrix} \underline{v}^{B*} \\ \underline{\hat{v}}^{I*} \end{bmatrix} = H_H \begin{bmatrix} \underline{v}^{B*} \\ \dot{\underline{q}} \end{bmatrix}. \tag{33}$$

If the elastic component features more than one boundary point, it can be readily shown that this relationship still holds, provided that the elastic motions at the boundary points remain small. Note the close parallel between Herting's transformation for displacements and velocities, eqs. (8) and (33), respectively. Although Herting's transformation, eq. (8), is a linearized relationship inherently associated with the small displacement assumption, the corresponding transformation for velocities, eq (33), is valid for total velocities (involving both small "elastic" and large "rigid" velocities), under the same small displacement assumption.

Using eq. (33), the kinetic energy of the fuselage, eq. (29), becomes

$$\mathcal{K} = \frac{1}{2} \begin{bmatrix} \underline{v}^{B*} \\ \dot{\underline{q}} \end{bmatrix}^T \bar{M} \begin{bmatrix} \underline{v}^{B*} \\ \dot{\underline{q}} \end{bmatrix}. \tag{34}$$

The inertial forces $\underline{\mathcal{F}}^i$ are readily found from variations of the kinetic energy

$$\delta\mathcal{K} = \begin{bmatrix} \delta\underline{x}^B \\ \delta\underline{\psi}^B \\ \hline \delta\underline{q} \end{bmatrix}^T \begin{bmatrix} (R^B R_0\,\underline{h}^*)^{\cdot} \\ (R^B R_0\,\underline{g}^*)^{\cdot} + \dot{\underline{x}}^B R^B R_0\,\underline{h}^* \\ \dot{\underline{h}}^q \end{bmatrix} = \begin{bmatrix} \delta\underline{x}^B \\ \delta\underline{\psi}^B \\ \hline \delta\underline{q} \end{bmatrix}^T \underline{\mathcal{F}}^i, \tag{35}$$

where

$$\begin{bmatrix} \underline{h}^* \\ \underline{g}^* \\ \underline{h}^q \end{bmatrix} = \bar{M} \begin{bmatrix} \underline{v}_B^* \\ \underline{\omega}_B^* \\ \dot{\underline{q}} \end{bmatrix}, \tag{36}$$

are the momenta components.

Consider an elastic fuselage featuring a single boundary point. If no modes are selected in Herting's transformation, the fuselage is effectively modeled as a rigid body. The reduced mass matrix becomes

$$\bar{M} = \begin{bmatrix} I \\ G^{IB} \end{bmatrix}^T M \begin{bmatrix} I \\ G^{IB} \end{bmatrix} = M_{RR}. \tag{37}$$

Since in this case G^{IB} stores the value of rigid body motion at the interior points the component, M_{RR} becomes the exact 6×6 mass matrix for the rigid fuselage. In other words, the formulation exactly reproduces rigid body dynamics when the elasticity of the fuselage is inhibited. Note that when more than one boundary point is used, elasticity is inherent to the formulation, even when no elastic modes are selected.

The evaluation of the kinetic energy of the modal based element only requires the reduced mass matrix $\bar{M} = H_H^T M H_H$; hence, it is independent of the finite element code used to model the elastic fuselage.

4.4 Discretization of the Elastic and Inertial Forces

Due to the complex dynamical behavior of multibody systems, it is desirable to used robust time integration methods (Refs. [35, 36, 37]) that present nonlinear unconditional stability characteristics. Let t_i and t_f denote the initial and final instants of a time step, respectively. The subscripts $(\cdot)_i$ and $(\cdot)_f$ then indicate the value of a specific quantity at times t_i and t_f, respectively. The following discretization of the elastic forces is proposed

$$\underline{\mathcal{F}}^e_m = \begin{bmatrix} - & R^F_m R_0 \, \underline{f}^u_m \\ - & T_m \, \underline{f}^\theta_m - \tilde{u}_m \, R^F_m R_0 \, \underline{f}^u_m \\ & R^F_m R_0 \, \underline{f}^u_m \\ & T_m \, \underline{f}^\theta_m \\ & \underline{f}^q_m \end{bmatrix}, \tag{38}$$

where the subscript $(\cdot)_m = 1/2\,[(\cdot)_i + (\cdot)_f]$ indicates an averaged quantity, *e.g.* $R^F_m = (R^F_f + R^F_i)/2$. $T_m = 1/2\,[\underline{h}_{32m} - \underline{h}_{23m},\ \underline{h}_{13m} - \underline{h}_{31m},\ \underline{h}_{21m} - \underline{h}_{12m}]$ where $\underline{h}_{\alpha\beta m} = \tilde{e}^F_{\alpha m}\, \underline{e}^B_{\beta m}$. The following discretization of the inertial forces is proposed

$$\underline{\mathcal{F}}^i_m = \frac{1}{\Delta t} \begin{bmatrix} (R^B R_0 \, \underline{h}^*)_f - (R^B R_0 \, \underline{h}^*)_i \\ (R^B R_0 \, \underline{g}^*)_f - (R^B R_0 \, \underline{g}^*)_i + (\tilde{x}^B_f - \tilde{x}^B_i)\left(R^B R_0 \, \underline{h}^*\right)_m \\ \underline{h}^q_f - \underline{h}^q_i \end{bmatrix}, \tag{39}$$

where $\Delta t = t_f - t_i$. It is then readily shown that the work done by the elastic forces during one time step is $\Delta \mathcal{W}^e = \mathcal{V}_f - \mathcal{V}_i$, and that the work done by the inertial forces is $\Delta \mathcal{W}^i = \mathcal{K}_f - \mathcal{K}_i$. Consequently, in the absence of external loads, the equations of motion of the modal element imply $\mathcal{E}_f = \mathcal{K}_f + \mathcal{V}_f = \mathcal{K}_i + \mathcal{V}_i = \mathcal{E}_i$, *i.e.* the total mechanical $\mathcal{E}$ energy of the system is preserved. This energy preservation guarantees nonlinear unconditional stability of the time integration process and it can be readily extended to an energy decaying formulation by following the steps outlined in section 4.3 of Reference [35].

4.5 Choice of the Floating Frame

The strain and kinetic energies of the modal based element were developed in previous sections for a general kinematic configuration that involves a floating frame. Note that the floating frame explicitly appears in the expression of the strain energy, but not in that of the kinetic energy. In order to implement the proposed formulation, a specific floating frame must be selected. The easiest choice is to attach the floating frame at a boundary point. This is readily achieved by Boolean identification of the corresponding degrees of freedom in the expression of the elastic forces, eq. (21). The inertial forces derived in eq. (35) can be used without modification. For a moving floating frame, the location and orientation of the floating frame become a function of the other degrees of freedom of the model, and hence, are eliminated from the formulation (Ref. [14]).

5 Numerical Examples

The following examples validate the proposed formulation. In all the examples a body-attached floating frame was used.

5.1 Crank-Panel Mechanism

The first example deals with the crank-panel mechanism shown in fig. 2. The mechanism consists of a 1 m $\times$ 1 m panel connected to two reinforcing beams along the opposite edges **AD** and **BC**.

The reinforcing beam along edge **AD** is connected to the ground by means of two revolute joints at points **A** and **D**, respectively. A spherical joint connects the other reinforcing beam to a push rod at point **B**. The push rod is connected to a crank by means of a universal joint at point **E**. Finally, a revolute joint connects the crank to the ground at point **O**, and the relative rotation at this joint is denoted ϕ. The mechanism is initially at rest and the root rotation of the crank is prescribed as

$$\phi(t) = \begin{cases} \pi/4\ (1 - \cos \pi t/T), & t \leq T, \\ \pi/2, & t > T, \end{cases} \tag{40}$$

The physical properties of the system were as follows: crank length $\ell_C = 0.25$ m, push rod length $\ell_P = 1.0$ m and panel thickness $h = 15$ mm. The entire mechanism is made of aluminum: Young's modulus $E = 73$ GPa, Poisson's ratio $\nu = 0.3$, and density $\rho = 2,700$ kg/m^3. All beams present square cross-sections: 40 mm $\times$ 40 mm for both the crank and push rod; 60 mm $\times$ 60 mm and 30 mm $\times$ 30 mm for the reinforcing beams along the **AD** and **BC** edges, respectively.

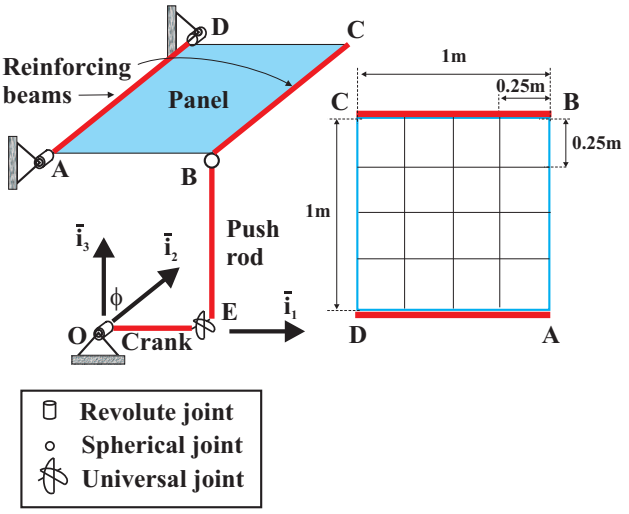

Figure 2: Configuration of the crank-panel mechanism.

Several cases were considered. *Case 1A* is the baseline case where no modal reduction was performed. The panel was modeled with 16 quadratic shell elements (Ref [38]) forming the 4×4 mesh shown in fig. 2. The reinforcing beams were modeled with four quadratic beam elements, and the push rod and crank by three and two quadratic elements, respectively. In *case 2A*, the elastic component consisting of the panel and reinforcing beams was modeled by a modal based element featuring four boundary nodes at the four corners of the panel. Eight bending modes were used in the reduction, with boundary conditions corresponding to clamped conditions at points **A** and **D**. If the Craig-Bampton method had been used, it would have been required to use boundary conditions for the selected modes corresponding to clamped conditions at all boundary nodes, *i.e.* at points **A**, **B**, **C**, and **D**. With the proposed Herting transformation, arbitrary boundary conditions may be used, in particular those corresponding to clamped conditions at points **A** and **D** and free conditions at points **B** and **C** which are more representative of the deformation patterns expected to occur during operation. The body-attached frame was located at point **A**. In both cases, the crank period was set to $T = 0.2$ sec and a constant time step $\Delta t = 3 \times 10^{-4}$ sec was used in the simulations. *Cases 1B* and *2B* are identical to *1A* and *2A*, respectively, except for the crank period which was reduced to $T = 0.05$ sec. A constant time step $\Delta t = 1 \times 10^{-4}$ sec was used.

Figure 3 shows the displacements and velocities of the panel at point **C** for *cases 1A* and *2A*. Excellent agreement is observed between the predictions of the full finite element and modal based simulations. Figure 4 depicts the push rod mid-span axial force and crank mid-span bending moment. No appreciable differences are observed between the full finite element and modal based simulations.

In the next set of simulations, the crank period was shortened to $T = 0.05$ sec. Due to the increased driving force, and system velocities and accelerations, the crank reached its final position more rapidly and nonlinear effects became more pronounced. Figure 5 depicts the displacements and velocities of the panel at point **C** for emphcases 1B and *2B*. The full finite element and modal based simulations are in fair agreement during the early stages of the simulation, up to $t = 0.05$ sec. At this time, the crank reaches its final position $\phi = \pi/2$ rad and the discrepancies between

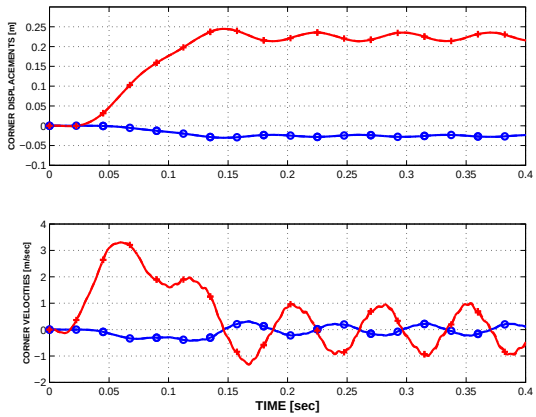

Figure 3: Time history of the vertical (+) and horizontal (∘) panel displacements (top graph) and velocities (bottom graph) at point **C**. *Case 1A*: solid line (full finite element model); *case 2A*: dashed-dotted line (reduced model). Period of the crank $T = 0.2$ sec.

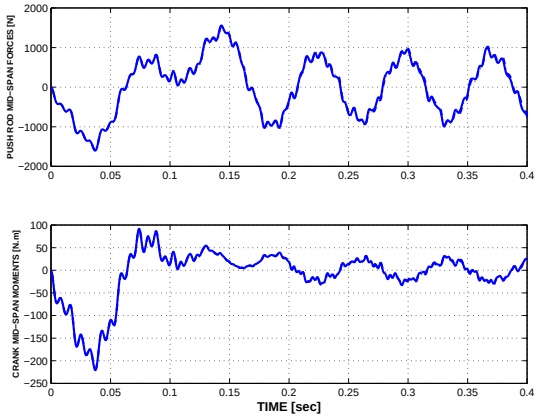

Figure 4: Time history of push rod mid-span axial force (top graph) and crank mid-span bending moment (bottom graph). *Case 1A*: solid line (full finite element model); *case 2A*: dashed-dotted line (reduced model). Period of the crank $T = 0.2$ sec.

the predictions of the two models become more pronounced. Figure 6 depicts the push rod mid-span axial force and crank mid-span bending moment. The full finite element simulation predicts a 3,200 N.m peak-to-peak crank mid-span moment as compared to 2,100 N.m for the modal based approach, a 35% reduction. Doubling the number of modes used in *case 2B* did not reduce the discrepancies between the two models. Hence, the observed discrepancies are due to large elastic motion effects, not to modal truncation.

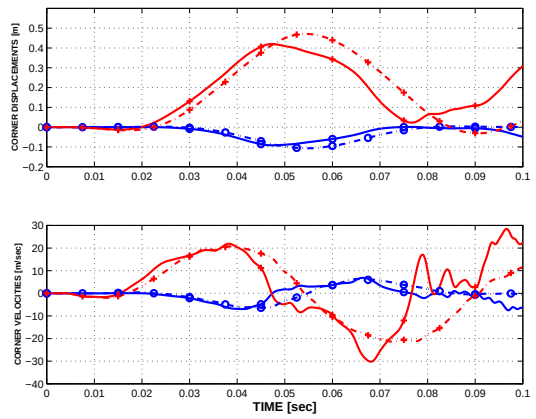

Figure 5: Time history of the vertical (+) and horizontal (∘) panel displacements (top graph) and velocities (bottom graph) at point **C**. *Case 1B*: solid line (full finite element model); *case 2B*: dashed-dotted line (reduced model). Period of the crank $T = 0.05$ sec.

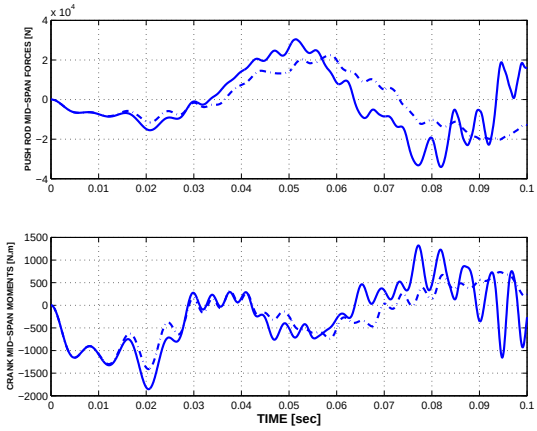

Figure 6: Time history of push rod mid-span axial force (top graph) and crank mid-span bending moment (bottom graph). *Case 1B*: solid line (full finite element model); *case 2B*: dashed-dotted line (reduced model). Period of the crank $T = 0.05$ sec.

5.2 Rotor-Fuselage Analysis

Next, a practical example is described: Sikorsky's UH-60 rotor connected to a stick model of the fuselage. The rotor physical properties are described in Reference [39] and references therein.

Figure 7 shows the helicopter configuration used in the present simulation. A revolute joint connects the main rotor to the fuselage. Each blade was modeled using six cubic beam elements, and the flap, lag, and pitching hinges by revolute joints. The stick model of the fuselage consisted of an assembly of 47 cubic beam elements (Refs. [35, 36, 37]) and 48 rigid bodies featuring a total of 512 degrees of freedom. The aerodynamic forces acting on the system were computed based on the unsteady, two-dimensional airfoil theory developed by Peters (Ref. [40]), and the three-dimensional unsteady inflow model developed by the same author (Ref. [41]). During the simulation, the control inputs were set to the following values, termed standard control inputs: collective $\theta_0 = 10.7$ deg, longitudinal cyclic $\theta_s = -4.9$ deg, lateral cyclic $\theta_c = 4.7$ deg. The helicopter was in a forward flight at a speed of $U = 150$ ft/sec.

The stick model used in this study is not expected to be detailed enough to provide an accurate model of the dynamic behavior of the fuselage. However, the focus of the study is the validation of the proposed modal based element. With the simple stick model, it is possible to solve the coupled rotor/fuselage dynamics problems in two different manners. First, the coupled problem is solved using a full finite element model, *i.e* without resorting to a modal formulation for the fuselage. The computational cost of a simulation with a very complete and detailed finite element model of the fuselage would be prohibitive. Next, the same problem is solved using the modal based representation of the fuselage. Comparison between the predictions of both models will validate the proposed formulation and determine its range of validity.

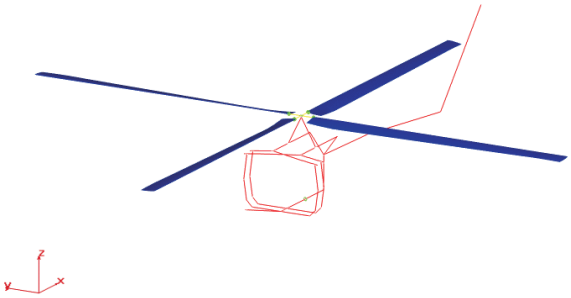

Figure 7: Configuration of the rotor-fuselage system.

Three cases, denoted *cases 1A* through *3A* were considered. *Case 1A* is the baseline case. The hub was clamped to the ground and no fuselage model was used in the simulation. In *case 2A*, the rotor was connected to a full finite element model of the stick representation of the fuselage which was clamped at the center of mass of the helicopter. *Case 3A* is identical to *case 2A* except that the full finite element model of the fuselage was replaced by a modal based element featuring two boundary nodes located at the hub and center of mass of the fuselage,respectively.

Forty modes were used in the reduction, with boundary conditions corresponding to free-free conditions. These modes are the forty lowest modes of the fuselage and cover a frequency range from 0 to 12P. The simulations were run for several main rotor revolutions until a periodic solution was reached. The figures described below show the response of the rotor for one period, once the periodic solution is achieved.

Figure 9 shows the Fourier harmonics of the hub in-plane force expressed in the fixed system, at frequencies of 4, 8 and 12P. Clearly, significant differences are observed between *case 1A*, that corresponds to a fixed-hub condition, and *cases 2A* and *3A* that correspond to coupled rotor/fuselage models. The full finite element and modal based simulations are in good agreement. Similar results are observed in Fig. 8 which depicts the Fourier harmonics of the overturning moment expressed in the fixed system.

In the next set of simulations, a rolling maneuver was studied. The rolling angle ϕ was prescribed at a revolute joint that connected the fuselage center of mass to the ground. First, a periodic solution for straight level flight was reached; then, the roll angle was prescribed as

$$\phi(t) = \begin{cases} \pi/8\ (1 - \cos \pi t/T), & t \leq T, \\ \pi/4, & t > T. \end{cases} \tag{41}$$

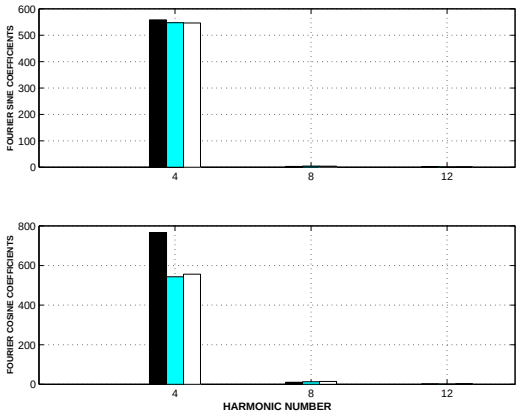

Figure 8: Fourier harmonics of the hub overturning moment expressed in the fixed system. *Case 1A*: black bars (isolated rotor); *case 2A*: gray bars (rotor/fuselage system, full finite element model) and *case 3A*: white bars (rotor/fuselage system, reduced model).

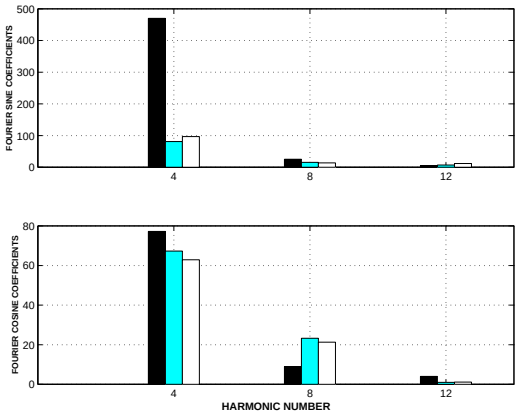

Figure 9: Fourier harmonics of the hub in-plane force expressed in the fixed system. *Case 1A*: black bars (isolated rotor); *case 2A*: gray bars (rotor/fuselage system, full finite element model) and *case 3A*: white bars (rotor/fuselage system, reduced model).

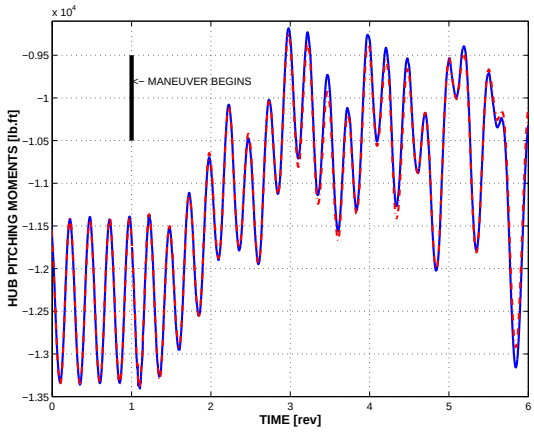

Figure 10: Time history of the hub pitching moment. *Case 2B*: solid line (rotor/fuselage system, full finite element model) and *case 3B*: dashed-dotted line (rotor/fuselage system, reduced model). Maximum roll rate of 1.06 rad/sec.

Clearly, this prescribed rotation generates a large angle maneuver, *i.e.* at the end of the maneuver the helicopter has rotated $\pi/4$ rad. The dynamic inflow model used here does not account for wake distortion effects and hence, is no longer valid for maneuvering flight. Consequently, the following figures present results of a qualitative nature.

Two cases were studied, denoted *case 2B* and *case 3B*. In *case 2B*, a full finite element model of the fuselage was used, whereas the proposed modal based element of the fuselage was used for *case 3B*. The modal basis was identical to that used in *case 3A*. The period of the roll maneuver, T, was set to $T = 5\ T_R$, where T_R is the period of the main rotor.

Figure 10 shows the time history of the hub pitching moment. The figure shows one complete revolution of level flight, for reference, followed by the five revolutions corresponding to the roll maneuver. Increased hub pitching moments are observed during the maneuver. Clearly, the agreement between the full finite element and modal based simulations is excellent.

The hub rolling moment was computed and reached a maximum value at $t \approx 4$ rev, *i.e.* when the maximum rolling rate of 1.06 rad/sec (≈ 60 deg/sec) is achieved, see eq. (41). The blade root twisting moment was also evaluated; at $t \approx 4$ rev, its peak-to-peak value reached a maximum value

which is about 38% higher than that of the periodic solution. Once again, the correlation between the predictions of the full finite element and modal based simulations was found to be excellent; the discrepancy was smaller than 1.5% at times during the maneuver.

In the final set of simulations, two cases, denoted *case 2C* and *case 3C*, were studied; these models are identical to *cases 2B* and *3B*, respectively, but the period of roll maneuver, T, was reduced to $T = 2.5\ T_R$, see eq. (41). This corresponds to a violent maneuver with a maximum rolling rate of 2.12 rad/sec ($\approx$ 120 deg/sec). Figure 12 depicts the time history of the hub pitching moment. Due to the higher roll rate, the peak pitching moments increase significantly for *cases 2C* and *3C* as compared to the predictions obtained for *cases 2B* and *3B*. Although the full finite element and modal based solutions are still in good agreement, it is apparent that their correlation starts to degrade for the faster roll rate. This discrepancy is probably due to the presence of nonlinear effects which cannot be captured by a modal approximation of the fuselage. Similar trends are observed in Fig. 11 that depicts the hub rolling moment. The present maneuver is at the limit of the maneuvering capabilities of the UH-60 aircraft; yet good agreement is observed between *case 2C* and *3C*. This indicates that the proposed modal reduction approach will yield good predictions even for the most violent maneuvers the aircraft can perform.

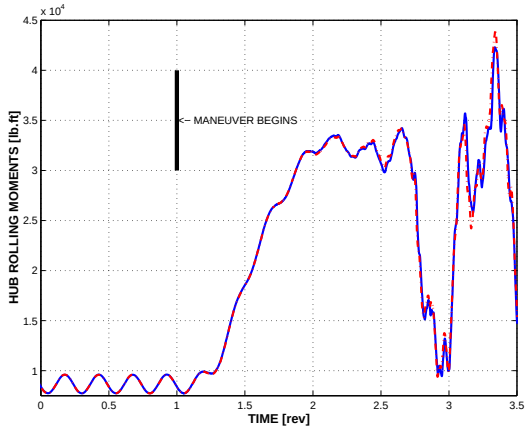

Figure 11: Time history of the hub rolling moment. *Case 2C*: solid line (rotor/fuselage system, full finite element model) and *case 3C*: dashed-dotted line (rotor/fuselage system, reduced model). Maximum roll rate of 2.12 rad/sec.

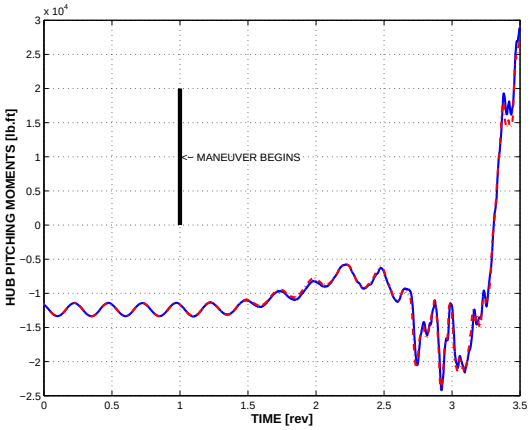

Figure 12: Time history of the hub pitching moment. *Case 2C*: solid line (rotor/fuselage system, full finite element model) and *case 3C*: dashed-dotted line (rotor/fuselage system, reduced model). Maximum roll rate of 2.12 rad/sec.

6 Conclusions

An approach to the modeling of coupled rotor/fuselage dynamics has been developed, based on component mode synthesis concepts. The proposed approach is based on Herting's transformation and presents attractive features. First, it allows the use of any modal basis for the fuselage. This contrasts with other approaches, such as those based on the Craig-Bampton of Rubin-MacNeal transformations that require specific boundary conditions for the selected modes. Second, the proposed approach can be used with a body-attached or moving frame; the body-attached frame was used in this work. Third, the fuselage model is readily coupled to other components of the rotorcraft through boundary nodes that retain physical degrees of freedom for this purpose. Fourth, the formulation recovers the exact equations of motion for a rigid fuselage in the absence of elastic deformations. Finally, the proposed approach is completely independent of the finite element package used to compute the modes of the fuselage.

The formulation was validated by comparing the predictions of full finite element models with those of the proposed modal based element. Excellent agreement was found between the predictions of both models in forward and maneuver flight. Good agreement was still found in the case of a violent maneuver. The proposed approach is based on the assumption of small elastic displacements; hence, its predictions are expected to degrade when large elastic displacements are present, resulting in nonlinear effects that are not captured by the proposed formulation. This validation of the predictions of modal based elements against those of full finite element models is an important step toward the development of robust rotor/fuselage dynamics models.

7 Acknowledgments

This work was sponsored by the Rotorcraft Industry Technology Association, under contract WBS No. 2002-B-01-01.1-A1. Dr. Yung Yu is the technical monitor.

References

[1] R.E. Hansford. Considerations in the development of the coupled rotor fuselage model. *Journal of the American Helicopter Society*, 39(4):70–81, 1994.

[2] H. Yeo and I. Chopra. Coupled rotor/fuselage vibration analysis for teetering rotor and test data comparison. *Journal of Aircraft*, 38:111–121, 2001.

[3] T-K. Hsu and D.A. Peters. Coupled rotor/airframe vibration analysis by a combined harmonic-balance, impedance matching method. *Journal of the American Helicopter Society*, 27:25–34, 1982.

[4] R. Gabel and V. Sankewitsch. Rotor-fuselage coupling by impedance. In *American Helicopter Society 42nd Annual Forum Proceedings*, Washington, D.C., June 1986.

[5] R.C. Cribbs, P.P. Friedmann, and Chiu T. Coupled helicopter rotor/flexible fuselage aeroelastic model for control of structural response. *AIAA Journal*, 38:1777–1788, 2000.

[6] W. Stephens and D.A. Peters. Rotor-body coupling revisited. *Journal of the American Helicopter Society*, 32:68–72, 1987.

[7] G. Bir and I. Chopra. Prediction of blade stresses due to gust loading. *Vertica*, 10:353–377, 1986.

[8] S. Vellaichamy and I. Chopra. Aeroelastic response of helicopters with flexible fuselage modeling. In *Proceedings of the 33rd Structures, Structural Dynamics and Materials Conference, Dallas, Texas, April, 1992*, 1992. AIAA Paper 92-2567.

[9] T.M. Wasfy and A.K. Noor. Computational strategies for flexible multibody systems. *ASME Applied Mechanics Reviews*, 56(2):553–613, 2003.

[10] A.A. Shabana. Flexible multibody dynamics: Review of past and recent developments. *Multibody System Dynamics*, 1(2):189–222, June 1997.

[11] R.G. Kvaternik. The NASA/Industry design analysis methods for vibrations (DAMVIBS) program - A government overview. In *Proceedings of the 33rd AIAA Structures, Structural Dynamics and Material Conference, Dallas, Texas, April 1992*, pages 1257–1262, 1992.

[12] A.A. Shabana. Substructure synthesis methods for dynamic analysis of multi-body systems. *Computers & Structures*, 20:737–744, 1985.

[13] A. Cardona and M. Géradin. Modelling of superelements in mechanism analysis. *International Journal for Numerical Methods in Engineering*, 32:1565–1593, 1991.

[14] A. Cardona and M. Géradin. A superelement formulation for mechanism analysis. *Computer Methods in Applied Mechanics and Engineering*, 100:1–29, 1992.

[15] O.P. Agrawal and A.A. Shabana. Application of deformable-body mean axis to flexible multibody system dynamics. *Computer Methods in Applied Mechanics and Engineering*, 56(2):217–245, 1986.

[16] A. Cardona. Superelements modelling in flexible multibody dynamics. *Multibody System Dynamics*, 4:245–266, 2000.

[17] A.A. Shabana. Resonance conditions and deformable body co-ordinate systems. *Journal of Sound and Vibration*, 192:389–398, 1996.

[18] P. Ravn. *Analysis and Synthesis of Planar Mechanical Systems Including Flexibility, Contact and Joint Clearance*. PhD thesis, Technical University of Denmark, 1998.

[19] L. Meirovitch. *Elements of Vibration Analysis*. McGraw-Hill Book Company, New York, 1975.

[20] J.A.C. Ambrósio and J.P.C. Gonçalves. Complex flexible multibody systems with application to vehicle dynamics. In Jorge A.C. Ambrósio and Werner O. Schiehlen, editors, *Advances in Computational Multibody Dynamics, IDMEC/IST, Lisbon, Portugal, Sept. 20-23, 1999*, pages 241–258, 1999.

[21] J.A.C. Ambrósio. Geometric and material nonlinear deformations in flexible multibody systems. In Jorge Ambrósio and Michal Kleiber, editors, *Proceedings of Computational Aspects of Nonlinear Structural Systems with Large Rigid Body Motion, NATO Advanced Research Workshop, Pultusk, Poland, July 2-7*, pages 91–115, 2000.

[22] R.R. Craig and M.C. Bampton. Coupling of substructures for dynamic analyses. *AIAA Journal*, 6:1313–1319, 1968.

[23] R.H. MacNeal. A hybrid method of component mode synthesis. *Computers & Structures*, 1(4):581–601, 1971.

[24] S. Rubin. Improved component-mode representation for structural dynamic analysis. *AIAA Journal*, 13:995–1006, 1975.

[25] D.N. Herting. A general purpose, multi-stage, component modal synthesis method. *Finite Elements in Analysis and Design*, 1:153–164, 1985.

[26] R.M. Hintz. Analytical methods in component modal synthesis. *AIAA Journal*, 13:1007–1016, 1975.

[27] R.R. Craig and C. Chang. Free-interface methods of substructure coupling for dynamic analysis. *AIAA Journal*, 14:1633–1635, 1976.

[28] W.S. Yoo and E.J. Haug. Dynamics of articulated structures. Part I. Theory. *Journal of Structural Mechanics*, 14:105–126, 1986.

[29] W.S. Yoo and E.J. Haug. Dynamics of articulated structures. Part II. Computer implementation and applications. *Journal of Structural Mechanics*, 14:177–189, 1986.

[30] W.S. Yoo and E.J. Haug. Dynamics of flexible mechanical systems using vibration and static correction modes. *Journal of Mechanisms, Transmissions, and Automation in Design*, 108:315–322, 1986.

[31] E.J. Wu, S. Haug. Geometric non-linear substructuring for dynamics of flexible mechanical elements. *International Journal for Numerical Methods in Engineering*, 26:2211–2226, 1988.

[32] A.A. Shabana and R.A. Wehage. A coordinate reduction technique for dynamic analysis of spatial substructures with large angular rotations. *Journal of Structural Mechanics*, 11(3):401–431, March 1983.

[33] R.J. Guyan. Reduction of stiffness and mass matrices. *AIAA Journal*, 3(2):380–385, 1965.

[34] K.J. Bathe. *Finite Element Procedures*. Prentice Hall, Inc., Englewood Cliffs, New Jersey, 1996.

[35] O.A. Bauchau. Computational schemes for flexible, nonlinear multi-body systems. *Multibody System Dynamics*, 2(2):169–225, 1998.

[36] O.A. Bauchau and C.L. Bottasso. On the design of energy preserving and decaying schemes for flexible, nonlinear multi-body systems. *Computer Methods in Applied Mechanics and Engineering*, 169(1-2):61–79, 1999.

[37] O.A. Bauchau, C.L. Bottasso, and L. Trainelli. Robust integration schemes for flexible multibody systems. *Computer Methods in Applied Mechanics and Engineering*, 192(3-4):395–420, 2003.

[38] O.A. Bauchau, J.Y. Choi, and C.L. Bottasso. On the modeling of shells in multibody dynamics. *Multibody System Dynamics*, 8(4):459–489, 2002.

[39] W.G. Bousman and T. Maier. An investigation of helicopter rotor blade flap vibratory loads. In *American Helicopter Society 48th Annual Forum Proceedings*, pages 977–999, Washington, D.C., June 3-5 1992.

[40] D.A. Peters, S. Karunamoorthy, and W.M. Cao. Finite state induced flow models. Part I: Two-dimensional thin airfoil. *Journal of Aircraft*, 32(2):313–322, 1995.

[41] D.A. Peters and C.J. He. Finite state induced flow models. Part II: Three-dimensional rotor disk. *Journal of Aircraft*, 32(2):323–333, 1995.